# ABSORPTION OSCILLATOR STRENGTHS FOR THE $c_4'^{1}\Sigma_u^+(3, 4, 6)–X^1\Sigma_g^+(v'')$, $b'^{1}\Sigma_u^+(10, 13, 20)–X^1\Sigma_g^+(v'')$, AND $c_5'^{1}\Sigma_u^+(1)–X^1\Sigma_g^+(v'')$ PROGRESSIONS IN $N_2$

C. LAVÍN AND A. M. VELASCO

Departamento de Química Física y Química Inorgánica, Facultad de Ciencias, Universidad de Valladolid, E-47011 Valladolid, Spain; clavin@qf.uva.es

## ABSTRACT

Absorption oscillator strengths, calculated with the molecular quantum defect orbital method, for the $c_4'^{1}\Sigma_u^+(3)–X^1\Sigma_g^+(v'' = 0\text{–}12)$, $c_4'^{1}\Sigma_u^+(4)–X^1\Sigma_g^+(v'' = 0\text{–}12)$, $c_4'^{1}\Sigma_u^+(6)–X^1\Sigma_g^+(v'' = 0\text{–}12)$, $b'^{1}\Sigma_u^+(10)–X^1\Sigma_g^+(v'' = 0\text{–}12)$, $b'^{1}\Sigma_u^+(13)–X^1\Sigma_g^+(v'' = 0\text{–}12)$, $b'^{1}\Sigma_u^+(20)–X^1\Sigma_g^+(v'' = 0\text{–}12)$, and $c_5'^{1}\Sigma_u^+(1)–X^1\Sigma_g^+(v'' = 0\text{–}12)$ bands of molecular nitrogen are reported. The Rydberg–valence interaction between states of $^{1}\Sigma_u^+$ symmetry has been treated through an interaction matrix that includes vibrational coupling. Due to the homogeneous interaction, the intensity distribution of the bands within each progression deviates from the Franck–Condon predictions. The present results for vibronic transitions from the $X^1\Sigma_g^+(0)$ ground state agree rather well with reported high-resolution measurements. As far as we know, $f$-values for bands originating from $v'' > 0$ vibrational levels of the electronic ground state are reported here for the first time. These data may be useful in the interpretation of the extreme ultraviolet spectra from Earth's and Titan's atmospheres, in which several bands of the $c_4'(3)$, $c_4'(4)$, and $c_4'(6)$ progressions have been identified.

Key words: molecular data – planets and satellites: atmospheres – ultraviolet: planetary systems

## 1. INTRODUCTION

The Rydberg and valence bands of molecular nitrogen are of considerable interest in the analysis of extreme ultraviolet (EUV) molecular emission observations in the atmospheres of Earth, Titan, and Triton, where $N_2$ is the dominant constituent (Strobel & Shemansky 1982; Broadfoot et al. 1989; Meier 1991). According to Ajello et al. (2007), the EUV spectrum of Titan's atmosphere obtained by the Ultraviolet Imaging Spectrometer (UVIS) on board *Cassini* consists of excitations from the $X^1\Sigma_g^+$ ground state to the $c_4'^{1}\Sigma_u^+$ Rydberg state and to the $b^1\Pi_u$ and $b'^{1}\Sigma_u^+$ valence states of $N_2$. In particular, bands belonging to the $c_4'^{1}\Sigma_u^+(v' = 3)–X^1\Sigma_g^+(v'')$, $c_4'^{1}\Sigma_u^+(v' = 4)–X^1\Sigma_g^+(v'')$, and $c_4'^{1}\Sigma_u^+ (v' = 6)–X^1\Sigma_g^+(v'')$ progressions, which are one of the main focuses of this work, have been detected in nitrogen-rich planetary atmospheres. Feldman et al. (2001) detected the $c_4'^{1}\Sigma_u^+(3)–X^1\Sigma_g^+(4)$ and $c_4'^{1}\Sigma_u^+(4)–X^1\Sigma_g^+(5)$ bands in the terrestrial airglow spectra obtained with the *Far Ultraviolet Spectroscopic Explorer* (*FUSE*). Strobel & Shemansky (1982) identified the $c_4'^{1}\Sigma_u^+(3)–X^1\Sigma_g^+(0, 2, 3)$ and $c_4'^{1}\Sigma_u^+(4)–X^1\Sigma_g^+(0)$ bands in Titan's EUV emission spectra obtained by the *Voyager 1* spacecraft. More recently, Ajello et al. (2007) performed an analysis of the EUV spectrum of Titan's atmosphere obtained by the UVIS on board *Cassini*. Their analysis revealed that the $c_4'^{1}\Sigma_u^+(3)–X^1\Sigma_g^+(2\text{–}5)$, $c_4'^{1}\Sigma_u^+(4)–X^1\Sigma_g^+(1, 3\text{–}6)$, and $c_4'^{1}\Sigma_u^+(6)–X^1\Sigma_g^+(4, 5, 7, 8)$ bands are present in EUV spectra of Titan's atmosphere. On the other hand, the $c_4'^{1}\Sigma_u^+(3)–X^1\Sigma_g^+(2\text{–}4)$, $c_4'^{1}\Sigma_u^+(4)–X^1\Sigma_g^+(3\text{–}5)$ and $c_4'^{1}\Sigma_u^+(6)– X^1\Sigma_g^+(8)$ bands have been observed in the spectrum of Mars obtained by Krasnopolsky & Feldman (2002) using FUSE. The interpretation of the spectral observations obtained with FUSE and *Cassini* requires the knowledge of $N_2$ radiative parameters such as lifetimes, band oscillator strengths, and predissociation rates (Liu & Shemansky 2006; Liu et al. 2008; Huber et al. 2009).

Several studies have been performed on spectroscopic properties of the $c_4'^{1}\Sigma_u^+(3)$, $c_4'^{1}\Sigma_u^+(4)$, and $c_4'^{1}\Sigma_u^+(6)$ states.

Absorption and emission spectra of bands belonging to the Rydberg $c_4'^{1}\Sigma_u^+–X^1\Sigma_g^+$ system have been photographed at high-resolution (Carroll & Yoshino 1972; Yoshino et al. 1979; Roncin et al. 1987, Roncin et al. 1991). Lifetime measurements of the $c_4'^{1}\Sigma_u^+(3)$ and $c_4'^{1}\Sigma_u^+(4)$ states have been performed by Kam et al. (1989) and Helm et al. (1993), respectively. For these states, predissociation yields have also been measured (Walter et al. 1994; Ajello et al. 1998). Moreover, perturbations in the photoexcitation and predissociation of $c_4'^{1}\Sigma_u^+(3)$ and $c_4'^{1}\Sigma_u^+(4)$ states have been investigated by Walter et al. (2000) using photofragment spectroscopy. Emission cross-sections for $v''$ progression from $c_4'^{1}\Sigma_u^+(3)$, $c_4'^{1}\Sigma_u^+(4)$, and $c_4'^{1}\Sigma_u^+(6)$ have been measured at medium- (Ajello et al. 1989) and high-resolution (Heays et al. 2014). Oscillator strengths, or $f$-values, for the $c_4'^{1}\Sigma_u^+(3)–X^1\Sigma_g^+(0)$, $c_4'^{1}\Sigma_u^+(4)–X^1\Sigma_g^+(0)$, and $c_4'^{1}\Sigma_u^+(6)–X^1\Sigma_g^+(0)$ bands have been derived from the relative electron scattering spectra of Geiger & Schröder (1969) by Zipf & McLaughlin (1978), from electron impact measurements (Ajello et al. 1989), and from electron energy loss measurements (Chan et al. 1993). More recently, $f$-values obtained from high-resolution measurements of the rotational lines have been reported for the $c_4'^{1}\Sigma_u^+(3)–X^1\Sigma_g^+(0)$ (Stark et al. 2008), $c_4'^{1}\Sigma_u^+(4)–X^1\Sigma_g^+(0)$ (Heays et al. 2009), and $c_4'^{1}\Sigma_u^+(6)–X^1\Sigma_g^+(0)$ (Huber et al. 2009) bands.

Absorption oscillator strengths for transitions to the $c_4'^{1}\Sigma_u^+(3)$, $c_4'^{1}\Sigma_u^+(4)$, and $c_4'^{1}\Sigma_u^+(6)$ from $v'' > 0$ vibrational levels of the electronic ground state, to our knowledge, have not been reported to data despite $f$-values being important for interpreting molecular spectra. In the present work, we have calculated absorption oscillator strengths for the $c_4'^{1}\Sigma_u^+(3)–X^1\Sigma_g^+(0\text{–}12)$, $c_4'^{1}\Sigma_u^+(4)–X^1\Sigma_g^+(0\text{–}12)$, and $c_4'^{1}\Sigma_u^+(6)–X^1\Sigma_g^+(0\text{–}12)$ bands of $N_2$ with the molecular quantum defect method (MQDO). This method has proved to be reliable for dealing with electronic and rotational line intensities in the EUV spectrum of molecular nitrogen (Lavín et al. 2004, 2008, 2010; Lavín & Velasco 2011). It is well known that the $N_2 c_4'^{1}\Sigma_u^+$ Rydberg

state is homogeneously perturbed by valence and Rydberg states of $^1\Sigma_u^+$ symmetry (Yoshino et al. 1979). Hence, in our calculations of oscillator strengths, we have taken into account the coupling between the three lowest states of $^1\Sigma_u^+$ symmetry. For this, we have employed a theoretical model of Rydberg–valence interaction that has been previously used to estimate transition intensities for mixed states in NO (Bustos et al. 2004; Velasco et al. 2010). The present calculations indicate strong interactions between the $c_4'^{\,1}\Sigma_u^+(3)$ and $b'^{1}\Sigma_u^+(10)$ states, $c_4'^{\,1}\Sigma_u^+(4)$ and $b'^{1}\Sigma_u^+(13)$ states, and among $c_4'^{\,1}\Sigma_u^+(6)$, $b'^{1}\Sigma_u^+$ (20), and $c_5'^{\,1}\Sigma_u^+(1)$ states, in accord with previous predictions (Stahel et al. 1983). As a result of the vibronic coupling, the bands belonging to the $c_4'^{\,}\Sigma_u^+(3, 4, 6)$–$X(v'')$ progressions can lose or gain intensity. In order to analyze the transfer of intensity between the $c_4'^{1}\Sigma_u^+$–$X^1\Sigma_g^+, b'^{\,\,1}\Sigma_u^+$–$X^1\Sigma_g^+$, and $c_5'^{\,1}\Sigma_u^+$–$X^1\Sigma_g^+$ systems, we have also calculated absorption oscillator strengths for the $b'^{1}\Sigma_u^+(10, 13, 20)$–$X^1\Sigma_g^+(0\text{–}12)$, and $c_5'^{\,1}\Sigma_u^+(1)$–$X^1\Sigma_g^+(0\text{–}12)$ bands. In this context, Stevens et al. (2011) have recently addressed the importance of the study of the exchange of intensity between the $c_4'^{1}\Sigma_u^+$–$X^1\Sigma_g^+$ and $b'^{1}\Sigma_u^+$–$X^1\Sigma_g^+$ systems for the interpretation of Titan's atmosphere spectra.

## 2. METHOD OF CALCULATION

In the electric dipole approximation, the absorption oscillator strength for a transition from a bound vibrational level $v''$ of the lower electronic state into a vibrational level $v'$ of the upper electronic state is defined as (Larsson 1983)

$$f_{v'v''} = \frac{8\pi^2 mca_0^2}{3h}\nu_{v'v''}\left|\left\langle v'\left|R_e\right|v''\right\rangle\right|^2, \tag{1}$$

where $\nu_{v'v''}$ is the wavenumber of the band origin in $cm^{-1}$, and $R_e$ is the electronic transition moment (in atomic units). The integral in Equation (1) can be written as a product of independent vibrational and electronic factors:

$$\left|\left\langle v'\left|R_e\right|v''\right\rangle\right|^2 = q_{v'v''}R_e^2. \tag{2}$$

Here $q_{v'v''}$ is the Franck–Condon factor, which is given by the square of the overlap integral of the vibrational wave functions of the two electronic states involved in the transition. In this work we have used the Rydberg–Klein–Rees (RKR) method to determine the potential energy curves. From these potential energies, the rotationless vibrational wave functions—and hence $q_{v'v''}$—are then obtained by solving the Schrö-dinger equation with the Numerov algorithm.

Equation (2) is appropriate when both the lower and upper states are unperturbed. However, if the upper state is perturbed by interaction with other vibrational levels—which occurs in $N_2$—the factorization is no longer possible. In order to include the homogeneous interaction between the Rydberg and valence states of $^1\Sigma_u^+$ symmetry in the calculation of transition moments, we have followed a perturbation model that has previously been described in detail (Bustos et al. 2004). Briefly, for each state, the wave function is a linear combination $|e_0, v_0\rangle$ of the unperturbed wave functions $|e, v_e\rangle$,

$$|e_0, v_0\rangle = \sum_{e=1}^{ne}\sum_{v_e=0}^{v_{e,\max}}|e, v_e\rangle C_{v_e, v_0}, \tag{3}$$

where $ne$ is the number of electronic states considered in the interaction, $v_e$ is the vibrational level of the electronic state $e$, and $v_{e,\max}$ is the highest vibrational level of the electronic state $e$. The perturbation coefficients are obtained by diag-onalization of a vibronic interaction matrix whose diagonal elements are the energies of the unperturbed states and whose off diagonal elements are the coupling parameters. The expression for the vibronic transition moment from a non-perturbed $|X, 0\rangle$ to the mixed $|e_0, v_0\rangle$ state is:

$$\langle M_{v_0 0}\rangle = \sum_{e=1}^{ne}\sum_{v_e=0}^{v_{e,\max}}C_{v_0, v_e}^* R_e S_{v_e 0}^{eX}, \tag{4}$$

where $S_{v_e 0}^{eX}$ is the vibrational overlap integral.

By introducing the last expression into Equation (1), we have

$$f_{v'v''} = \frac{8\pi^2 mca_0^2}{3h}\nu_{v'v''}\left[\sum_{e=1}^{ne}\sum_{v_e=0}^{v_{e,\max}}C_{v_0, v_e}^* R_e S_{v_e 0}^{eX}\right]^2. \tag{5}$$

In this work, the electronic transition moment for Rydberg transitions has been calculated with the MQDO method, which has been described in detail elsewhere (Martín et al. 1996, 2001). In this approach, the radial part of the MQDO wave functions is derived by analytically solving the Schrödinger equation, formulated in terms of a one-electron Hamiltonian with a parametric potential of the form:

$$V(r) = \frac{(c - \delta)(2l + c - \delta + 1)}{2r^2} - \frac{1}{r}, \tag{6}$$

where $\delta$ is the quantum defect for a given molecular state and $c$ is an integer with a narrow range of values that ensure the normalizability of the wave functions. The angular part of the MQDO wave functions is a symmetry-adapted linear combination of spherical harmonics, so that the complete MQDO's form bases for the different irreducible representations of the molecular point group, $D_{\infty h}$ in the case of $N_2$. One of the main advantages of this method is that it yields analytical expressions for the transition integrals and thus of oscillator strengths, avoiding potential convergence problems.

## 3. RESULTS AND DISCUSSION

Molecular nitrogen has a closed shell electronic configuration in its $^1\Sigma_g^+$ ground state: $(1\sigma_g)^2(1\sigma_u)^2(2\sigma_g)^2(2\sigma_u)^2(1\pi_u)^4(3\sigma_g)^2$. Focusing on excited electronic states of $^1\Sigma_u^+$ symmetry, the valence $b'^{1}\Sigma_u^+$ and the Rydberg $c_4'^{\,1}\Sigma_u^+$ and $c_5'^{\,1}\Sigma_u^+$ states are prominent in the EUV spectrum of $N_2$. The excited $c_4'^{\,1}\Sigma_u^+$ and $c_5'^{\,1}\Sigma_u^+$ states correspond to the two lowest members of the $np\sigma$ Rydberg series that converges into the $X^2\Sigma_g^+$ ground state of the cationic core $N_2^+$ (Carroll & Yoshino 1972).

In order to calculate oscillator strengths, we have taken into account the interaction between vibrational levels of the three $^1\Sigma_u^+$ states: the valence state $b'^{1}\Sigma_u^+$ ($v = 0$–27) and the Rydberg states $c_4'^{\,1}\Sigma_u^+$ ($v = 0$–8) and $c_5'^{\,1}\Sigma_u^+$ ($v = 0$–2). The electronic interaction energies used in the interaction matrix are those reported by Stahel et al. (1983). For the calculation of the vibrational overlap integrals with the RKR model, we have used the molecular constants given by Edwards et al. (1993) for the $X^1\Sigma_u^+$ ground state and by Stahel et al. (1983) for the $c_4'^{\,1}\Sigma_u^+$, $c_5'^{\,\,1}\Sigma_u^+$, and $b'^{1}\Sigma_u^+$ excited states. The electronic

**Table 1**
Main Components of Wave Functions for the $c_4'{}^1\Sigma_u^+(3, 4, 6)$, $b'{}^1\Sigma_u^+$ (10, 13, 20), and $c_5'{}^1\Sigma_u^+$ (1) Vibronic States (Coefficients $\geqslant |0.10|$)

| Vibronic State | Wave Function Components | | | | | | |
|---|---|---|---|---|---|---|---|
| $c_4'$ 3 | 0.83 ($c_4'$ 3) | −0.48 ($b'$ 10) | −0.16 ($b'$ 11) | −0.10 ($b'$ 12) | ⋯ | ⋯ | ⋯ |
| $c_4'$ 4 | 0.85 ($c_4'$ 4) | −0.45 ($b'$ 13) | −0.15 ($b'$ 14) | −0.10 ($b'$ 15) | 0.10 ($c_5'$ 1) | ⋯ | ⋯ |
| $c_4'$ 6 | 0.94 ($c_4'$ 6) | 0.16 ($c_5'$ 1) | −0.14 ($b'$ 20) | −0.13 ($c_5'$ 0) | −0.11 ($b'$ 21) | −0.10 ($b'$ 18) | ⋯ |
| $b'$ 10 | 0.87 ($b'$ 10) | 0.47 ($c_4'$ 3) | −0.10 ($b'$ 11) | ⋯ | ⋯ | ⋯ | ⋯ |
| $b'$ 13 | 0.88 ($b'$ 13) | 0.45 ($c_4'$ 4) | ⋯ | ⋯ | ⋯ | ⋯ | ⋯ |
| $b'$ 20 | 0.90 ($b'$ 20) | −0.31 ($c_5'$ 1) | 0.21 ($c_4'$ 6) | −0.12 ($b'$ 19) | ⋯ | ⋯ | ⋯ |
| $c_5'$ 1 | 0.61 ($b'$ 21) | 0.56 ($c_5'$ 1) | −0.43 ($b'$ 22) | 0.18 ($b'$ 20) | −0.15 ($b'$ 23) | 0.14 ($c_4'$ 7) | 0.11 ($b'$ 19) |

**Table 2**
Franck–Condon Factors for the $c_4'{}^1\Sigma_u^+–X^1\Sigma_g^+$, $b'{}^1\Sigma_u^+–X^1\Sigma_g^+$, and $c_5'{}^1\Sigma_u^+–X^1\Sigma_g^+$ Transitions of $N_2$

| $X^1\Sigma_g^+$ | $c_4'{}^1\Sigma_u^+$ | | | $b'{}^1\Sigma_u^+$ | | | $c_5'{}^1\Sigma_u^+$ |
|---|---|---|---|---|---|---|---|
| $v''$ | $v' = 3$ | $v' = 4$ | $v' = 6$ | $v' = 10$ | $v' = 13$ | $v' = 20$ | $v' = 1$ |
| 0 | 0.000 | 0.000 | 0.000 | 0.035 | 0.081 | 0.055 | 0.079 |
| 1 | 0.015 | 0.001 | 0.000 | 0.068 | 0.041 | 0.048 | 0.756 |
| 2 | 0.221 | 0.029 | 0.000 | 0.042 | 0.000 | 0.007 | 0.157 |
| 3 | 0.436 | 0.264 | 0.006 | 0.002 | 0.031 | 0.020 | 0.008 |
| 4 | 0.289 | 0.312 | 0.071 | 0.014 | 0.022 | 0.013 | 0.000 |
| 5 | 0.038 | 0.331 | 0.307 | 0.035 | 0.000 | 0.007 | 0.000 |
| 6 | 0.002 | 0.058 | 0.126 | 0.013 | 0.022 | 0.018 | 0.000 |
| 7 | 0.000 | 0.004 | 0.369 | 0.001 | 0.018 | 0.000 | 0.000 |
| 8 | 0.000 | 0.000 | 0.109 | 0.023 | 0.000 | 0.017 | 0.000 |
| 9 | 0.000 | 0.000 | 0.011 | 0.022 | 0.019 | 0.006 | 0.000 |
| 10 | 0.000 | 0.000 | 0.001 | 0.001 | 0.016 | 0.006 | 0.000 |
| 11 | 0.000 | 0.000 | 0.000 | 0.012 | 0.000 | 0.014 | 0.000 |
| 12 | 0.000 | 0.000 | 0.000 | 0.026 | 0.017 | 0.000 | 0.000 |

transition moments for $c_4'{}^1\Sigma_u^+–X^1\Sigma_g^+$ and $c_5'{}^1\Sigma_u^+–X^1\Sigma_g^+$ have been calculated with the MQDO methodology. For the $b'{}^1\Sigma_u^+–X^1\Sigma_g^+$ transition, we have used the electronic transition moment reported by Stahel et al. (1983). For our calculations, we need the ionization energy of a $N_2$ molecule and the energies of the Rydberg $c_4'{}^1\Sigma_u^+$ and $c_5'{}^1\Sigma_u^+$ states as input. In the present work, these data have been taken from Huber & Jungen (1990).

In Table 1 we displayed the main eigenvector components of the $c_4'{}^1\Sigma_u^+(v = 3, 4,$ and $6)$, $b'{}^1\Sigma_u^+(v = 10, 13,$ and $20)$, and $c_5'{}^1\Sigma_u^+(v = 1)$ vibronic states that are the subject of this work. Contributions that are less than an absolute value of 0.10 are not included. Our calculations show that the $c_4'{}^1\Sigma_u^+(3)$ Rydberg and $b'{}^1\Sigma_u^+(10)$ valence states are highly mixed with each other. A substantial mixing of the Rydberg $c_4'{}^1\Sigma_u^+(4)$ and valence $b'{}^1\Sigma_u^+(13)$ states is observed from Table 1. Concerning the $b'{}^1\Sigma_u^+$ (20) valence state, it is perturbed mainly by the $c_5'{}^1\Sigma_u^+$ (1) and $c_4'{}^1\Sigma_u^+(6)$ Rydberg states. As can be seen from Table 1, the electronic character of the conventionally named $c_5'{}^1\Sigma_u^+$ Rydberg state is predominantly $b'{}^1\Sigma_u^+$. These results are in agreement with earlier predictions (Stahel et al. 1983). The Franck–Condon factors presently obtained from the RKR approximation are given in Table 2.

The perturbed MQDO absorption oscillator strengths for the Rydberg $c_4'{}^1\Sigma_u^+$ ($v' = 3, 4, 6$)–$X^1\Sigma_g^+(v'' = 0$–$12)$ and $c_5'{}^1\Sigma_u^+$ ($v' = 1$)–$X^1\Sigma_g^+(v'' = 0$–$12)$ bands, and the valence $b'{}^1\Sigma_u^+(v' = 10, 13, 20)$–$X^1\Sigma_g^+(0$–$12)$ bands are listed together with $f$-values derived from experimental measurements (Zipf & McLaughlin 1978; Ajello et al. 1989; Chan et al. 1993; Stark et al. 2008; Heays et al. 2009; Huber et al. 2009) in

Tables 3 and 4. To simplify notation, we will omit, from now on, the lower state $X^1\Sigma_g^+$ and the symmetry of the upper electronic state to denote bands; for instance, we will use the notation $c_4'(3, 4)$ to denote the $c_4'{}^1\Sigma_u^+(3)$–$X^1\Sigma_g^+(4)$ band. As already mentioned, in the literature we have only found comparative $f$-values for vibronic transitions from the $X^1\Sigma_g^+(0)$ ground state, despite the spectroscopic properties of $N_2$ having been intensively investigated in the last few decades. In order to analyze the perturbation effects, the $f$-values calculated with non-mixed transition moments, Equation (2), are also included in Tables 3 and 4.

The unperturbed MQDO absorption oscillator strengths for the $c_4'(3, 0)$, $c_4'(4, 0)$, and $c_4'(6, 0)$ bands are extremely weak due to the poor Franck–Condon overlap between the vibronic upper $c_4'(v' = 3, 4, 6)$ states and the $X(0)$ ground state. Our calculations with mixed transition moments reveal that the $b'–X(0)$ contributions to the vibronic transition momentum completely dominate the oscillator strengths for the above bands. Therefore, the $c_4'(3, 0)$, $c_4'(4, 0)$, and $c_4'(6, 0)$ bands borrow their intensities from the $b'(10,0)$, $b'(13, 0)$ and $b'(20, 0)$ bands, respectively. On the other hand, the decrease in the intensity of the $c_5'(1, 0)$ band is significant. It can be explained in terms of the strong homogeneous interaction $b'–c_5'$. An overview of Tables 3 and 4 shows that the MQDO perturbed oscillator strengths for transitions toward the valence state $b'{}^1\Sigma_u^+$ and the two Rydberg states $c_4'{}^1\Sigma_u^+$ and $c_5'{}^1\Sigma_u^+$ from the $X^1\Sigma_g^+$ (0) ground state are in very good agreement with the recent $f$-values obtained from high-resolution measurements (Stark et al. 2008; Heays et al. 2009; Huber et al. 2009) for most bands. The close agreement between MQDO $f$-values obtained with mixed transition moments and recent

**Table 3**

Absorption Oscillator Strengths for the Rydberg $c_4'^1\Sigma_u^+(v'=3, 4, 6)-X^1\Sigma_g^+(v'')$ and $c_5'^1\Sigma_u^+(v'=1)-X^1\Sigma_g^+(v'')$ Progressions of $N_2$

| | $c_4'^1\Sigma_u^+(3)$ Progression | | | | $c_4'^1\Sigma_u^+(4)$ Progression | | | | $c_4'^1\Sigma_u^+(6)$ Progression | | | | $c_5'^1\Sigma_u^+(1)$ Progression | | |
| | Oscillator Strength | | | | Oscillator Strength | | | | Oscillator Strength | | | | | | |
| $v''$ | MQDO[a] | MQDO[b] | Expt | Emission Cross Section[c] | MQDO[a] | MQDO[b] | Expt | Emission Cross Section[c] | MQDO[a] | MQDO[b] | Expt | Emission Cross Section[c] | MQDO[a] | MQDO[b] | Expt |
|---|---|---|---|---|---|---|---|---|---|---|---|---|---|---|---|
| 0 | 0.0000 | 0.0062 | 0.0078(8)[d] 0.0136[f] 0.019[h] 0.0207[i] | 2.4 | 0.0000 | 0.0205 | 0.018(2)[e] 0.0285[f] 0.0496[h] 0.0592[i] | 4.6 | 0.0000 | 0.0056 | 0.0117(10)[e] 0.0179[f] 0.0135[h] 0.0176[i] | 3.5 | 0.0030 | 0.0003 | 0.00044(7)[g] |
| 1 | 0.0022 | 0.0037 | ... | 3.2 | 0.0002 | 0.0065 | ... | 5.1 | 0.0000 | 0.0087 | ... | 2.1 | 0.0281 | 0.0047 | ... |
| 2 | 0.0307 | 0.0485 | ... | 14 | 0.0042 | 0.0011 | ... | 0.51 | 0.0000 | 0.0005 | ... | 1.00 | 0.0057 | 0.0015 | ... |
| 3 | 0.0592 | 0.0338 | ... | 7.5 | 0.0366 | 0.0475 | ... | 24 | 0.0008 | 0.0000 | ... | ... | 0.0003 | 0.0003 | ... |
| 4 | 0.0385 | 0.0403 | ... | 16 | 0.0424 | 0.0159 | ... | 5.5 | 0.0100 | 0.0133 | ... | 6.0 | 0.0000 | 0.0023 | ... |
| 5 | 0.0050 | 0.0090 | ... | 4.2 | 0.0439 | 0.0341 | ... | 18 | 0.0425 | 0.0395 | ... | 12 | 0.0000 | 0.0007 | ... |
| 6 | 0.0003 | 0.0001 | ... | ... | 0.0075 | 0.0118 | ... | 8.3 | 0.0171 | 0.0112 | ... | 2.5 | 0.0000 | 0.0048 | ... |
| 7 | 0.0000 | 0.0012 | ... | 0.50 | 0.0005 | 0.0012 | ... | 1.3 | 0.0488 | 0.0377 | ... | 17 | 0.0000 | 0.0001 | ... |
| 8 | 0.0000 | 0.0013 | ... | 0.79 | 0.0000 | 0.0002 | ... | ... | 0.0141 | 0.0117 | ... | 6.3 | 0.0000 | 0.0041 | ... |
| 9 | 0.0000 | 0.0001 | ... | ... | 0.0000 | 0.0007 | ... | 0.90 | 0.0014 | 0.0010 | ... | ... | 0.0000 | 0.0043 | ... |
| 10 | 0.0000 | 0.0003 | ... | ... | 0.0000 | 0.0001 | ... | ... | 0.0001 | 0.0000 | ... | ... | 0.0000 | 0.0000 | ... |
| 11 | 0.0000 | 0.0009 | ... | 0.26 | 0.0000 | 0.0001 | ... | ... | 0.0000 | 0.0000 | ... | ... | 0.0000 | 0.0017 | ... |
| 12 | 0.0000 | 0.0004 | ... | ... | 0.0000 | 0.0005 | ... | ... | 0.0000 | 0.0000 | ... | ... | 0.0000 | 0.0000 | ... |

**Notes.**
[a] MQDO, with unperturbed transition moment.
[b] MQDO, with perturbed transition moment.
[c] Heays et al. (2014). Emission cross-sections at 100 eV, in units of $10^{-20}$ cm$^2$.
[d] Stark et al. (2008). The experimental error is given in parentheses.
[e] Heays et al. (2009). The experimental error is given in parentheses.
[f] Ajello et al. (1989).
[g] Huber et al. (2009). The experimental error is given in parentheses.
[h] Chan et al. (1993).
[i] Zipf & McLaughlin (1978).

**Table 4**
Absorption Oscillator Strengths for the Valence $b'^1\Sigma_u^+(v' = 10, 13, 20)$–$X^1\Sigma_g^+(v'')$ Progressions of $N_2$

| $v''$ | $b'^1\Sigma_u^+(10)$ Progression | | | $b'^1\Sigma_u^+(13)$ Progression | | | $b'^1\Sigma_u^+(20)$ Progression | | |
| | MQDO[a] | MQDO[b] | Expt | MQDO[a] | MQDO[b] | Expt | MQDO[a] | MQDO[b] | Expt |
|---|---|---|---|---|---|---|---|---|---|
| | | | 0.0042(4)[c] | | | | | | 0.0118(13)[d] |
| | | | 0.001643[e] | | | 0.010(1)[f] | | | 0.018373[e] |
| 0 | 0.0081 | 0.0029 | 0.0022[g] | 0.0190 | 0.0087 | 0.004443[e] | 0.0133 | 0.0088 | 0.0173[g] |
| | | | 0.0017[h] | | | 0.00455[h] | | | 0.0177[h] |
| 1 | 0.0153 | 0.0084 | | 0.0095 | 0.0036 | | 0.0113 | 0.0205 | |
| 2 | 0.0093 | 0.0013 | | 0.0001 | 0.0018 | | 0.0017 | 0.0005 | |
| 3 | 0.0004 | 0.0197 | | 0.0068 | 0.0024 | | 0.0046 | 0.0044 | |
| 4 | 0.0030 | 0.0016 | | 0.0046 | 0.0199 | | 0.0030 | 0.0000 | |
| 5 | 0.0072 | 0.0036 | | 0.0001 | 0.0052 | | 0.0015 | 0.0001 | |
| 6 | 0.0027 | 0.0039 | | 0.0046 | 0.0016 | | 0.0039 | 0.0061 | |
| 7 | 0.0002 | 0.0000 | | 0.0035 | 0.0031 | | 0.0000 | 0.0002 | |
| 8 | 0.0044 | 0.0036 | | 0.0000 | 0.0000 | | 0.0034 | 0.0022 | |
| 9 | 0.0042 | 0.0047 | | 0.0036 | 0.0035 | | 0.0011 | 0.0002 | |
| 10 | 0.0002 | 0.0006 | | 0.0030 | 0.0030 | | 0.0012 | 0.0019 | |
| 11 | 0.0021 | 0.0012 | | 0.0000 | 0.0000 | | 0.0028 | 0.0018 | |
| 12 | 0.0045 | 0.0039 | | 0.0030 | 0.0027 | | 0.0000 | 0.0002 | |

**Notes.**
[a] MQDO, with unperturbed transition moment.
[b] MQDO, with perturbed transition moment.
[c] Stark et al. (2008). The experimental error is given in parentheses.
[d] Huber et al. (2009). The experimental error is given in parentheses.
[e] Ajello et al. (1989).
[f] Heays et al. (2009). The experimental error is given in parentheses.
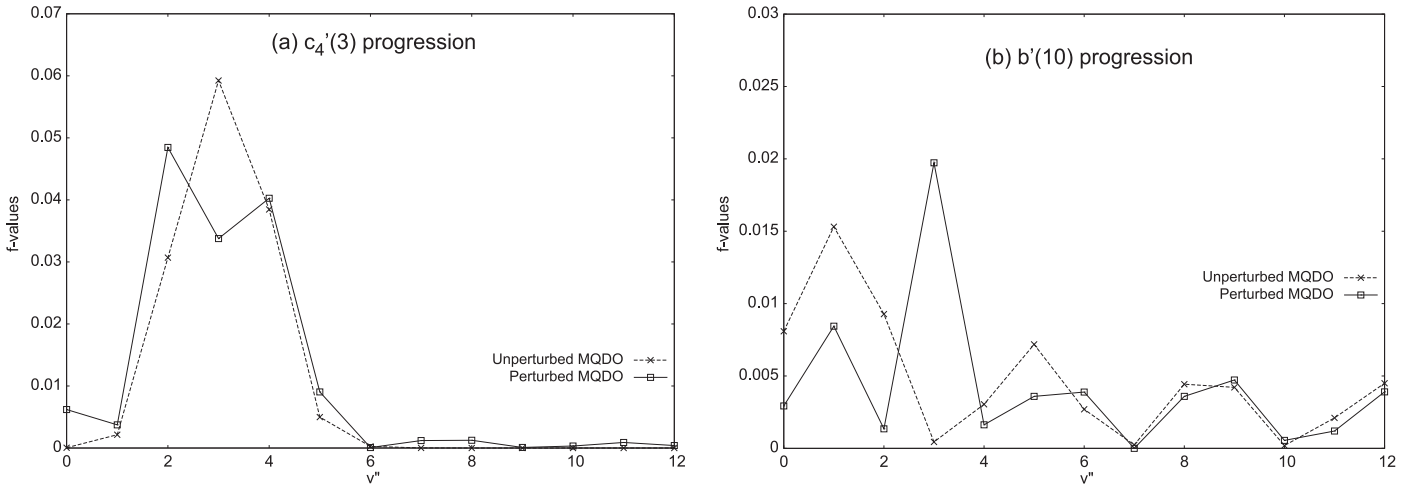[g] Chan et al. (1993).
[h] Zipf & McLaughlin (1978).



**Figure 1.** Absorption oscillator strengths as a function of the vibrational quantum number $v''$ for the (a) $c_4'^1\Sigma_u^+(3)$–$X^1\Sigma_g^+(v'')$ and (b) $b'^1\Sigma_u^+(10)$–$X^1\Sigma_g^+(v'')$ progressions of $N_2$.

experimental results indicates that the procedure used in this work adequately accounts for the valence–Rydberg mixing, so it is valid for predicting absorption intensities.

The band intensity distribution in the $c_4'^1\Sigma_u^+$–$X^1\Sigma_g^+$, $b'^1\Sigma_u^+$–$X^1\Sigma_g^+$, and $c_5'^1\Sigma_u^+$–$X^1\Sigma_g^+$ systems, as it is known, deviates from a normal Franck–Condon type intensity pattern due to the interaction. Later in this section, we discuss the perturbation effects in the intensity distribution for the vibrational progressions investigated here. In order to more clearly visualize the irregular vibronic intensities pattern shown by progressions, perturbed and unperturbed MQDO $f$-values are displayed in Figures 1–3.

As mentioned above, calculations of the electronic character of the $c_4'(3)$ and $b'(10)$ states using the previously described diabatic state mixing model reveal that these states are highly mixed with each other. The effects of the mutual interaction in the intensity distribution of the $c_4'(3)$–$X(v'')$ and $b'(10)$–$X(v'')$ vibrational progressions can be appreciated in Figures 1(a) and (b), respectively, where large departures from Franck–Condon predictions are observed in both progressions. Without the perturbation, the Franck–Condon factors would predict that the $c_4'(3, 3)$ band should be the strongest band in the $v' = 3$ progression. However, our calculations predict the $c_4'(3, 2)$ and $c_4'(3, 4)$ to be the most intense bands. The weakening of the
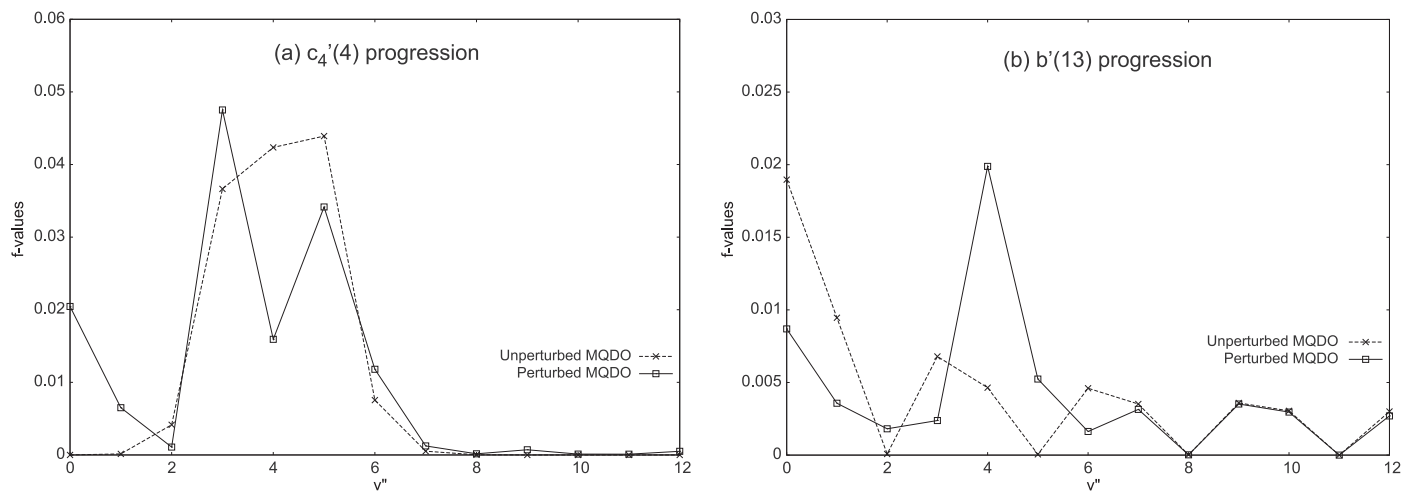
**Figure 2.** Absorption oscillator strengths as a function of the vibrational quantum number $v''$ for the (a) $c_4'\,^1\Sigma_u^+(4)$–$X^1\Sigma_g^+(v'')$ and (b) $b'^1\Sigma_u^+(13)$–$X^1\Sigma_g^+(v'')$ progressions of $N_2$.
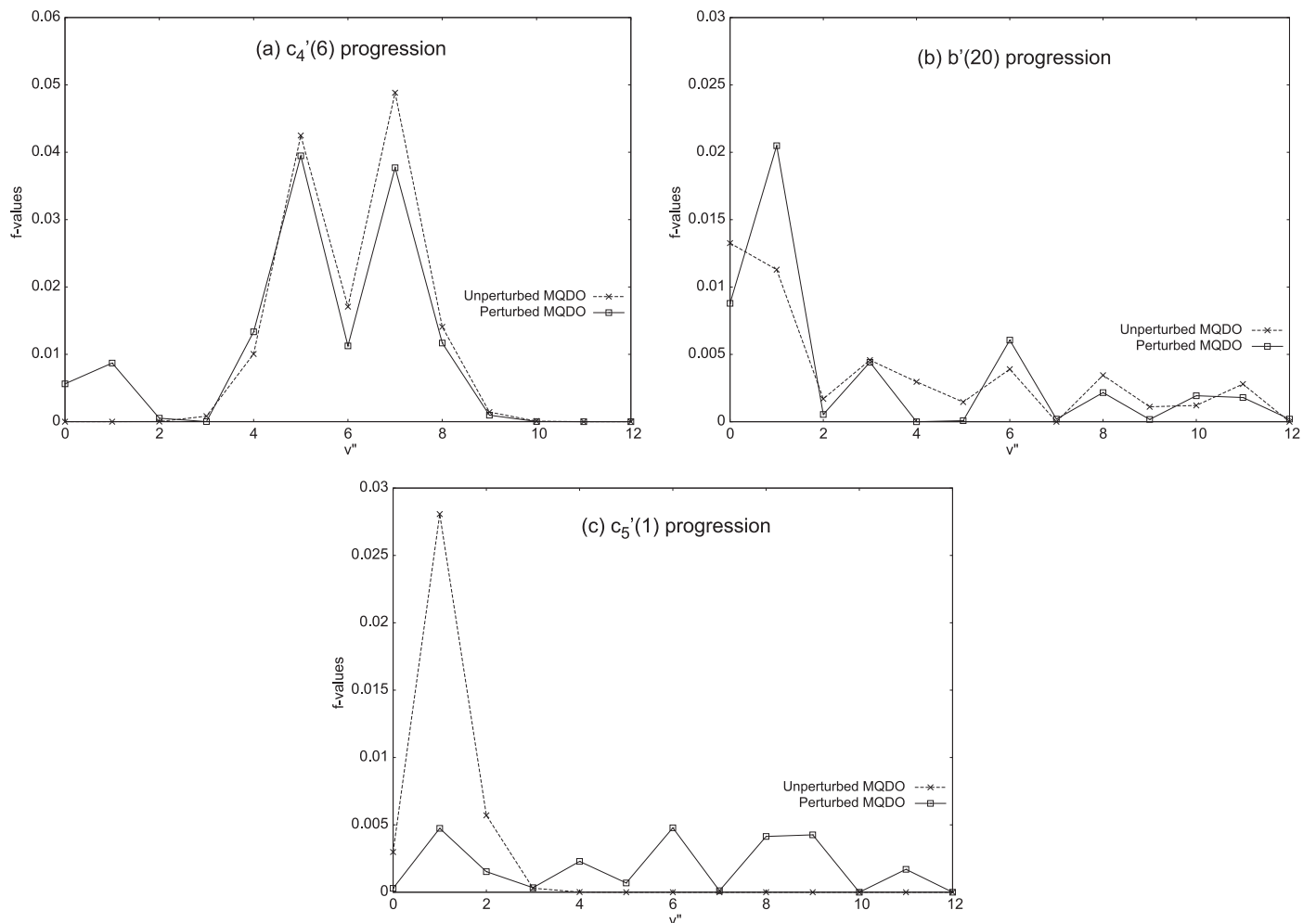


**Figure 3.** Absorption oscillator strengths as a function of the vibrational quantum number $v''$ for the (a) $c_4'\,^1\Sigma_u^+(6)$–$X^1\Sigma_g^+(v'')$, (b) $b'^1\Sigma_u^+(20)$–$X^1\Sigma_g^+(v'')$, and (c) $c_5'$ $^1\Sigma_u^+(1)$–$X^1\Sigma_g^+(v'')$ progressions of $N_2$.

intensity of the $c_4'(3, 3)$ band is a consequence of the perturbing effect of the $b'(10)$ valence state. The perturbed oscillator strengths calculated with Equation (5) involve either the sum or the difference of terms corresponding to the various vibrational levels that contribute to the transition moment. Therefore, the

homogeneous interaction can lead to constructive or destructive interference in the band $f$-value. The present calculations reveal that the coupling $c_4'(3)$–$b'(10)$ causes destructive interference in the $c_4'(3, 3)$ band and therefore a decrease of its $f$-value. Regarding the $b'(10)$–$X(v'')$ progression, the $b'(10, 3)$ is the

strongest band in spite of an unfavorable Franck–Condon factor. It should be mentioned that the largest contribution to the $b'(10)$–$X(3)$ transition moment comes, not from the unperturbed $b'(10)$ state itself, but rather from the diabatic $c_4'(3)$ state, owing to the better vibrational overlap of the latter with $X(3)$. Thus, the increase in the oscillator strength of the valence $b'(10, 3)$ band can be attributed to intensity borrowing from the Rydberg $c'(3, 3)$ band.

The Rydberg $c_4'(4)$ vibronic state is strongly mixed with the valence $b'$ state, mainly $b'(13)$. Our calculations predict an irregular vibronic intensity pattern for the $c_4'(4)$–$X(v'')$ and $b'(13)$–$X(v'')$ progressions, as is evident from Figures 2(a) and (b), where perturbed and unperturbed MQDO $f$-values for both progressions are plotted. It can also be observed in Figure 2(a) where there is a decrease of the intensity of the $c_4'(4, 4)$ absorption band and an increase of the $b'(13, 4)$ band when interaction is considered in the model. The analysis of the $c_4'$ and $b'$ contributions to the transition moment for these bands reveals that the coupling $c_4'(4)$–$b'(13)$ is destructive for the $c_4'(4, 4)$ band but constructive for the $b'(13, 4)$ band. In fact, the $b'(13, 4)$ band is the strongest band in the $b'(13)$–$X(v'')$ progression even though the $b'(13, 0)$ should be, by far, the strongest band from Franck–Condon considerations. The most intense absorption bands of the $c_4'(4)$–$X(v'')$ progression, that is, the $c_4'(4, 1)$, $c_4'(4, 3)$, $c_4'(4, 4)$, $c_4'(4, 5)$, $c_4'(4, 6)$ vibronic bands have been detected from Titan's emissions (Ajello et al. 2007). A few comments about the $c_4'(4, 1)$ are appropriate. In the absence of the $c_4'(4)$–$b'(13)$ perturbation, the MQDO $f$-value is very weak for the $c_4'(4, 1)$ band due to an unfavorable Franck–Condon factor. Calculations with mixed transition moments predict the $c_4'(4, 1)$ band to be relatively strong, gaining its intensity from the $b'(13, 1)$ band. It seems that the $c_4'(4, 1)$ band becomes observable in the atmosphere of Titan only because of this mixing.

The three excited levels $c_4'(6)$, $c_5'(1)$ and $b'(20)$ are strongly coupled, as is inferred from Table 1. The non-perturbed and perturbed MQDO $f$-values for the $c_4'(6)$–$X(v'')$, $b'(20)$–$X(v'')$, and $c_5'(1)$–$X(v'')$ vibrational progressions are plotted in Figures 3 (a)–(c), respectively. In contrast to what is expected on the basis of the Franck–Condon factors, the $c_4'(6, 0)$ and $c_4'(6, 1)$ and $c_4'(6, 2)$ bands are relatively strong. The increase in the oscillator strengths corresponding to these bands is due to the perturbation exercised by $b'$ and $c_5'$ states; in fact, the transition moment for them is dominated by $b'$, mainly $b'(20)$, and at a minor extent, by $c_5'(1)$. For the remaining bands of the $c_4'(6)$–$X(v'')$ progression, the transition moment is dominated mainly by $c_4'$. According to our calculations, the $c_4'(6, 5)$ and $c_4'(6, 7)$ are the most intense bands in this progression. These bands, together with the $c_4'(6, 4)$ and $c_4'(6, 8)$ bands have been detected in the atmosphere of Titan (Ajello et al. 2007). Concerning the $v''$ vibrational progression from $b'(v' = 20)$ valence state, deviations from predictions based on the Franck–Condon principle are observed. The anomalous behavior of the $b'(20, 1)$ band can be attributed to the $b'(20)$–$c_5'(1)$ coupling, which causes a constructive interference. Thereby, the valence $b'(20, 1)$ grows in intensity at the expense of the Rydberg $c_5'(1, 1)$ band and indeed becomes the strongest band in the progression $b'(20)$–$X(v'')$. In Table 4 and Figure 3(b) the homogeneous interaction effect in the valence $b'(20, 4)$ band is noticeable. For this band, the $b'$ and $c_4'$ contributions to the transition moment are of comparable magnitude and opposite sign, leading to the almost complete disappearance of the band.

Finally, the $c_5'$ $^1\Sigma_u^+(1)$ state, according to our calculations, suffers strong homogeneous interaction with nearby vibrational levels of the $b'$ state, predominantly $b'(21)$ and $b'(22)$. A striking feature of the $c_5'(1)$–$X(v'')$ progression is a significant decrease of the absorption oscillator strength for the $c_5'(1, 1)$ band when perturbation is taken into account. Such a decrease is due to destructive interference $b'(19$–$22)$ and $c_5'$ $^1\Sigma_u^+(1)$. On the contrary, the bands originating from $v'' \geqslant 4$ are gaining significant strength with increasing $v''$, as can be seen in Table 3 and Figure 3(c).

In summary, using the MQDO method we have calculated absorption oscillator strengths for $c_4'{}^1\Sigma_u^+$ (3, 4, 6)–$X^1\Sigma_g^+(v'' = 0$–$12)$, $b'{}^1\Sigma_u^+(10, 13, 20)$–$X^1\Sigma_g^+(v'' = 0$–$12)$, and $c_5'$ $^1\Sigma_u^+$ (1)–$X^1\Sigma_g^+(v'' = 0$–$12)$ progressions in molecular nitrogen. Included in this set of progressions are several bands observed in emissions from the atmospheres of Earth and Titan. To the best of our knowledge, $f$-values for bands with $v'' > 0$ are reported here for the first time. The comparison between MQDO $f$-values obtained with non-mixed and mixed transition moments and experimental results, when available, suggest that the procedure used in this work properly takes into account the valence–Rydberg mixing. In addition, perturbed MQDO results and emission cross-section measurements, reported by Heays et al. (2014), display a similar vibrational dependence for $c_4'$ $^1\Sigma_u^+$ ($v' = 3$, 4, 6)–$X^1\Sigma_g^+(v'')$ progressions, as can be seen in Table 3. Emission from the $b'(10)$, $b'(13)$, and $b'(20)$ valence states has not been observed in laboratory fluorescence spectra (Ajello et al. 1989; Heays et al. 2014). However, our calculations predict the $b'$ $^1\Sigma_u^+(10, 13, 20)$–$X^1\Sigma_g^+$ ($v'' = 0$–$12$) bands to have appreciable excitation intensities. This seems to indicate that the absence in emission of the corresponding bands may be due to the strong predissociation of the $b'(10)$, $b'(13)$, and $b'(20)$ states. Indeed, the $b'$ $^1\Sigma_u^+$ state has been reported (Helm et al. 1993) to be predissociated by continuum states of triplet symmetry, mainly 2 $^3\Pi_u$. It is expected that the rotational structure of bands presently studied will be also influenced by the valence–Rydberg interaction. In previous calculations (Lavin & Velasco 2011) of oscillator strengths for rotational lines of the $c_4'{}^1\Sigma_u^+(3)$–$X^1\Sigma_g^+(v'' = 0$–$5)$ bands, it was observed that the intensity distribution of the rotational lines within each of the vibronic bands deviates from predictions based on Hönl–London factors.

We have analyzed the transfer of intensity between the $c_4'{}^1\Sigma_u^+$–$X^1\Sigma_g^+$, $b'$ $^1\Sigma_u^+$–$X^1\Sigma_g^+$, and $c_5'$ $^1\Sigma_u^+$–$X^1\Sigma_g^+$ systems due to the homogeneous interaction. Our calculations with mixed transition moments show that the $c_4'(3, 0)$, $c_4'(4, 0)$, and $c_4'(4, 1)$ bands are observable in N2-rich planetary atmospheres because of the $c_4'$–$b'$ interaction. Recently Stevens et al. (2011) performed a spectral analysis of *Cassini* UVIS observations of Titan's airglow, and found that the blended $(3, 2)+(4, 3)$ bands, near 945 Å, and the $(3, 4)+(4, 5)$ bands, near 985 Å, are the most prominent bands in $c_4'{}^1\Sigma_u^+$ ($v' = 3$, 4, 6)–$X^1\Sigma_g^+(v'')$ progressions. The present calculations are consistent with these results concerning the $v''$ progressions from $v' = 3$ and $v' = 4$; however, our calculations predict that $f$-values for the $c_4'(6, 5)$ and $c_4'(6, 7)$ bands are remarkably similar in magnitude to those for the $c_4'(3, 2)$, $c_4'(3, 4)$, $c_4'(4, 3)$, and $c_4'(4, 5)$ bands. These results agree with the UVIS EUV airglow spectra from Titan presented by Ajello et al. (2007). These authors attributed the strong Titan emission feature at 944 Å to the $c_4'(3, 2)$, $c_4'(4, 3)$, $c_4'(6, 5)$ together with $b'(9, 2)$ and $b'(16, 4)$ bands, and the strong feature at 987 Å to the $c_4'(3, 4)$, $c_4'(4, 5)$, and $c_4'(6, 7)$

bands. This suggests that members of the $c_4'{}^1\Sigma_u^+$ $(v' = 6)$–$X^1\Sigma_g^+(v'')$ progression should also be included in models of the EUV airglow of Titan.

## REFERENCES

Ajello, J. M., James, G. K., & Ciocca, M. 1998, JPhB, 31, 2437
Ajello, J. M., James, G. K., Franklin, B. O., & Shemansky, D. E. 1989, PhRvA, 40, 3524
Ajello, J. M., Stevens, M. H., Stewart, I., et al. 2007, GeoRL, 34, L24204
Broadfoot, A. L., Atreya, S. K., Bertaux, J. L., et al. 1989, Sci, 246, 1459
Bustos, E., Granucci, G., Persico, M., et al. 2004, JPCA, 108, 11279
Carroll, P. K., & Yoshino, K. 1972, JPhB, 5, 1614
Chan, W. F., Cooper, G., Sodhi, R. N. S., & Brion, C. E. 1993, CP, 170, 81
Edwards, S., Roncin, J. Y., Launay, F., & Rostas, F. 1993, JMoSp, 162, 257
Feldman, P. D., Sahnow, D. J., Kruk, J. W., Murphy, E. M., & Moos, H. W. 2001, JGR, 106, 8119
Geiger, J., & Schröder, B. 1969, JChPh, 50, 7
Heays, A. N., Ajello, J. M., Aguilar, A., Lewis, B. R., & Gibson, S. T. 2014, ApJS, 211, 28
Heays, A. N., Lewis, B. R., Stark, G., et al. 2009, JChPh, 131, 194308
Helm, H., Hazell, I., & Bjerre, N. 1993, PhRvA, 48, 2762
Huber, K. P., Chan, M. C., Stark, G., Ito, K., & Matsui, T. 2009, JChPh, 131, 084301
Huber, K. P., & Jungen, Ch. 1990, JChPh, 92, 850
Kam, A. W., Lawall, J. R., Lindsay, M. D., et al. 1989, PhRvA, 40, 1279
Krasnopolsky, V. A., & Feldman, P. D. 2002, Icar, 160, 86
Larsson, M. 1983, A&A, 128, 291
Lavín, C., Martín, I., Mayor, E., & Velasco, A. M. 2008, MolPh, 106, 929
Lavin, C., & Velasco, A. M. 2011, ApJ, 739, 16
Lavín, C., Velasco, A. M., & Martín, I. 2010, CPL, 487, 38
Lavín, C., Velasco, A. M., Martín, I., & Bustos, E. 2004, CPL, 394, 114
Liu, X., & Shemansky, D. E. 2006, ApJ, 645, 1560
Liu, X., Shemansky, D. E., Malone, C. P., et al. 2008, JGR, 113, A02304
Martín, I., Lavín, C., Pérez-Delgado, Y., Pitarch-Ruiz, J., & Sánchez-Marín, J. 2001, JPCA, 105, 9637
Martín, I., Lavín, C., Velasco, A. M., et al. 1996, CP, 202, 307
Meier, R. R. 1991, SSRv, 58, 1
Roncin, J. Y., Launay, F., Subtil, J. L., & Yoshino, K. 1991, P&SS, 39, 1301
Roncin, J. Y., Launay, F., & Yoshino, K. 1987, P&SS, 35, 267
Stahel, D., Leoni, M., & Dressler, K. 1983, JChPh, 79, 2541
Stark, G., Lewis, B. R., Heays, A. N., et al. 2008, JChPh, 128, 114302
Stevens, M. H., Gustin, J., Ajello, J. M., et al. 2011, JGR, 116, A05304
Strobel, D. F., & Shemansky, D. E. 1982, JGR, 87, 1361
Velasco, A. M., Lavín, C., Bustos, E., et al. 2010, JPCA, 114, 8450
Walter, C. W., Cosby, P. C., & Helm, H. 1994, PhRvA, 50, 2930
Walter, C. W., Cosby, P. C., & Helm, H. 2000, JChPh, 112, 4621
Yoshino, K., Freeman, D. E., & Tanaka, Y. 1979, JMoSp, 76, 153
Zipf, E. C., & McLaughlin, R. W. 1978, P&SS, 26, 449